Ultra-high-Q TE/TM dual-polarized photonic crystal nanocavities

Yinan Zhang,* Murray W. McCutcheon, Ian B. Burgess, and Marko Loncar

School of Engineering and Applied Sciences, Harvard University, Cambridge, Massachusetts 02138, USA
*Corresponding author: yinan@seas.harvard.edu

Received May 26, 2009; accepted July 26, 2009;
posted August 12, 2009 (Doc. ID 111846); published August 31, 2009

We demonstrate photonic crystal nanobeam cavities that support both TE- and TM-polarized modes, each with a Q factor greater than one million and a mode volume on the order of the cubic wavelength. We show that these orthogonally polarized modes have a tunable frequency separation and a high nonlinear spatial overlap. We expect these cavities to have a variety of applications in resonance-enhanced nonlinear optics.

OCIS codes: 140.3945, 230.5750, 190.4390.

Ultrahigh-Q-factor photonic crystal nanocavities, which are capable of storing photons within a cubic-wavelength-scale volume (V_{mod}), enable enhanced light–matter interactions and therefore provide an attractive platform for cavity quantum electrodynamics [1] and nonlinear optics [2–6]. In most cases, high Q/V_{mod} nanocavities are achieved with planar photonic crystal platform based on thin semiconductor slabs perforated with a lattice of holes. These structures favor TE-like polarized modes (the electric field in the central mirror plane of the photonic crystal slab is perpendicular to the air holes). In contrast, the TM-like polarized bandgap is favored in a lattice of high-aspect-ratio rods [7]. TM-like cavities have been designed in an air-hole geometry as well [8–10], but the Q factors of these cavities were limited to the order of 10^3. In addition, the lack of vertical confinement of these cavities results in large-mode volumes [8]. Though it is possible to employ surface plasmons to localize the light tightly in the vertical direction, the lossy nature of metal limits the Q to about 10^2 [10].

In this Letter, we report a one-dimensional (1D) photonic crystal nanobeam cavity design that supports an ultrahigh-Q ($Q>10^6$) TM-like cavity mode with $V_{\mathrm{mod}}\sim(\lambda/n)^3$. This cavity greatly broadens the applications of optical nanocavities. For example, it is well suited for photonic crystal quantum-cascade lasers, since the intersubband transition in quantum-cascade lasers is TM polarized [11–13]. We also demonstrate that our cavity simultaneously supports two ultrahigh-Q modes with orthogonal polarizations (one TE-like and one TM-like). The frequency difference of the two modes can be widely tuned while maintaining the high Q factor of each mode, which is of interest for applications in nonlinear optics.

Our design is based on a dielectric suspended ridge waveguide with an array of uniform holes of periodicity a and radius R, which forms a photonic crystal Bragg mirror, as shown in Fig. 1(a). The refractive index of the dielectric is set to $n=3.4$ (similar to Si and GaAs at $\sim 1.5\ \mu$m). We start with a ridge of height:width:period ratio of 3:1:1 ($d_x=a$, $d_y=3a$) and $R=0.3a$. Figure 1(b) shows the transverse profiles of the fundamental TM-like and TE-like modes (TM_{00} and TE_{00}) supported by the ridge waveguide. Using the 3D finite-difference time-domain (FDTD) method, the transmittance spectra are obtained of the TM_{00} and TE_{00} modes launched toward the Bragg mirror. Figure 1(c) shows the TM_{00} and TE_{00} bandgaps, respectively. It has also been shown experimentally that 1D photonic crystal nanobeam cavities have Q/V_{mod} ratios comparable with 2D systems [14–16].

Introducing a lattice grading to the periodic structure creates a localized potential for both TE- and TM-like modes. To optimize the mode Q factors, we apply the bandgap-tapering technique that is well-developed in previous work [17–19]. We use an eight-segment tapered section with holes (R_1–R_8) and a 12-period mirror section at each side. Two degrees of freedom are available for each tapered segment: the length (w_k) and the radius (R_k). We keep the ratio R_k/w_k fixed at each segment and then implement a linear interpolation of the grating constant ($2\pi/w_k$). When the central segment w_8 is set to $0.84a$, we obtain ultrahigh Qs and low-mode volumes for both TE- and TM-polarized modes ($Q_{\mathrm{TE}}=1.2\times10^6$, $Q_{\mathrm{TM}}=2.4\times10^6$; both mode volumes are equal to $1.2[\lambda/n]^3$), with free-space wavelengths $4.30a$ and $4.78a$, respec-

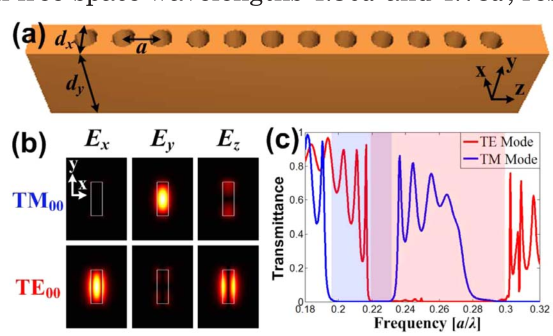

Fig. 1. (Color online) (a) Schematic of the nanobeam design, showing the nanobeam thickness (d_y) and width (d_x) and the hole spacing (a). (b) TE_{00} and TM_{00} transverse mode profiles for a ridge waveguide with $d_y=3d_x$. (c) Transmission spectra for the TE_{00} (light) and TM_{00} (dark) modes. The shaded areas indicate the bandgaps for both modes.

0146-9592/09/172694-3/$15.00

tively. Figures 2(b) and 2(c) show the mode profiles of the major components of the two modes in the xz mirror plane. The ultrahigh Q factors can also be interpreted in momentum space [8,20]. Figures 2(d) and 2(e) demonstrate the Fourier transformed (FT) profiles of the electric field components $E_{\mathrm{TE},x}$ and $E_{\mathrm{TM},y}$ in the xz plane ($y=0$), with the light cone indicated by the white circle. It can be seen that both modes' Fourier components are localized tightly at the bandedge of the Brillouin zone on the k_z axis ($k_z=\pi/a$). This reduces the amount of mode energy within the light cone that is responsible for scattering losses. It is also worthwhile to note that higher-longitudinal-order TE_{00} and TM_{00} cavity modes with different symmetry with respect to the xy mirror plane exist [19]. For example, the second-order TE_{00} mode, which has a node at the xy mirror plane, resonates at a wavelength of $4.43a$. It has a higher Q factor of 4.7×10^6 but a larger mode volume of $2.1(\lambda/n)^3$.

For a number of applications of interest, control of the frequency spacing between the two modes is required. Examples include polarization-entangled photon generation for degenerate modes [21] and terahertz generation for 0.1–10 THz mode splitting [4]. We tune the frequency separation of the two modes by varying the thickness of the structure while keeping the other parameters constant. In Fig. 3(a), the cavity resonances of the TE_{00} and TM_{00} modes are traced as a function of the nanobeam thickness (d_y/a). The TM-like modes have a much larger dependence on the thickness than the TE-like modes. The modes are degenerate at $d_y=1.26a$, and for thicknesses beyond this value, ω_{TE} is larger than ω_{TM}. As

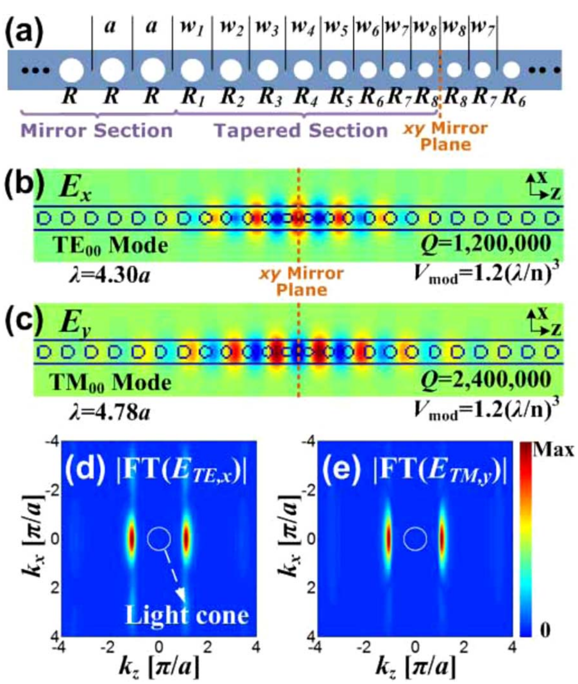

Fig. 2. (Color online) (a) Schematic of the 1D photonic crystal nanobeam cavity. (b), (c) Mode profiles of the electric field components $E_{\mathrm{TE},x}$ and $E_{\mathrm{TM},y}$ for the cavity design with $d_x=a$, $d_y=3a$. (d), (e) Spatial Fourier transform of the electric field component profiles ($E_{\mathrm{TE},x}$ and $E_{\mathrm{TM},y}$) in the xz plane ($y=0$).

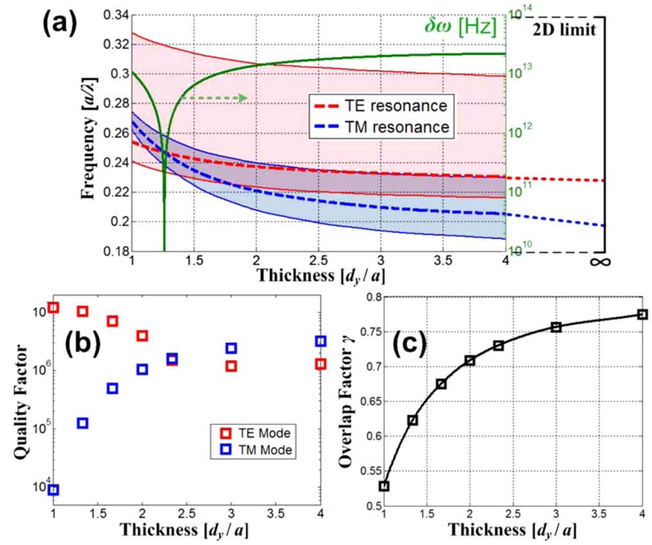

Fig. 3. (Color online) (a) TE_{00} (light) and TM_{00} (dark) cavity mode resonant frequencies (dotted curves) as a function of the nanobeam thickness. The bandgap regions of the two modes are shaded. The frequency separation ($\delta\omega$) of the two modes with the TE-like mode wavelength fixed at 1.5 μm is also plotted. (b), (c) Dependence of the Q factor and nonlinear overlap factor γ on the nanobeam thickness.

d_y increases, the splitting increases until it saturates when the system approaches the 2D limit (structure is infinite in the y direction). In this limit, we find that $\lambda_{\mathrm{TE}}=4.4a$ and $\lambda_{\mathrm{TM}}=5.1a$. The frequency separation ($\delta\omega=|\omega_{\mathrm{TE}}-\omega_{\mathrm{TM}}|$) of this design ranges from 0 to 20 THz, with the TE-like mode wavelength fixed at 1.5 μm by scaling the structure accordingly. Figure 3(b) shows the thickness dependence of the Q factor for the xz design specifications listed above. It can be seen that the Q factors of both TE- and TM-polarized modes stay above 10^5 for the $\omega_{\mathrm{TE}}>\omega_{\mathrm{TM}}$ branch.

Decreasing d_y causes the width of the TM bandgap to sharply decrease, whereas the width of the TE bandgap remains almost constant. The narrowed TM bandgap results in a reduced Bragg confinement, which increases the transmission losses through the Bragg mirrors. This is evidenced by the Q factor of the TM mode, which drops to 9000 when the thickness:width ratio is 1:1. Though this leakage can be compensated for, in principle, by increasing the number of periods of the mirror sections, the length of the structure also increases, which makes fabrication more challenging for a suspended nanobeam geometry. A narrow bandgap also leads to large penetration depth of the mode into the Bragg mirrors, thereby increasing the mode volume.

Next, we examine the application of our dual-polarized cavity for the resonance enhancement of nonlinear processes. To achieve a large nonlinear interaction in materials with dominant off-diagonal nonlinear susceptibility terms (e.g., $\chi^{(2)}_{ijk}, i\neq j\neq k$), such as III–V semiconductors [5], it is beneficial to mix two modes with orthogonal polarizations. As shown in our previous work [4], the strength of the nonlinear interaction can be characterized by the modal overlap, which can be quantified using the following figure of merit:

$$\gamma \equiv \epsilon_{r,d} \frac{\int_d \mathrm{d}^3\mathbf{r} \sum_{i,j,i\neq j} E_{\mathrm{TE},i} E_{\mathrm{TM},j}}{\sqrt{\int \mathrm{d}^3\mathbf{r}\epsilon_r |\mathbf{E}_{\mathrm{TE}}|^2} \sqrt{\int \mathrm{d}^3\mathbf{r}\epsilon_r |\mathbf{E}_{\mathrm{TM}}|^2}}, \quad (1)$$

where $\int_d$ denotes integration over only the regions of nonlinear dielectric and $\epsilon_{r,d}$ denotes the maximum dielectric constant of the nonlinear material. Note that we have normalized γ so that $\gamma=1$ corresponds to the theoretical maximum overlap. For the TE_{00} and TM_{00} modes we studied, the two major components ($E_{\mathrm{TE},x}$ and $E_{\mathrm{TM},y}$) share the same parity (have anti-nodes in all the three mirror planes), and only two overlap components, $E_{\mathrm{TE},x}E_{\mathrm{TM},y}$ and $E_{\mathrm{TE},y}E_{\mathrm{TM},x}$, in Eq. (1) do not vanish. This allows a large nonlinear spatial overlap. We obtain $\gamma=0.76$ for the cavity shown in Fig. 2. The overlap approaches $\gamma=0.78$ in the limit $d_y \rightarrow \infty$. We find that the overlap factor γ stays at a reasonably high value (>0.6) across the full range of the frequency difference tuning (for $\omega_{\mathrm{TE}} > \omega_{\mathrm{TM}}$ branch) [Fig. 3(c)].

Finally, it is important to note that thick nanobeams can support higher-order modes with a different number of nodes in the xy plane, as well. These higher-order modes are also confined in the tapered section within their respective bandgaps, with the Q factors and wavelengths listed in Fig. 4 for the $d_x=a$ and $d_y=3a$ cases. These modes can offer a broader spectral range than the fundamental modes, which is of great interest to nonlinear applications requiring a large bandwidth [5].

In conclusion, we have demonstrated that ultrahigh-Q TE- and TM-like fundamental modes with mode volumes $\sim(\lambda/n)^3$ can be designed in 1D photonic crystal nanobeam cavities. We have shown that the frequency splitting of these two modes can be tuned over a wide range without compromising the Q factors. We have also shown that these modes can have a high nonlinear overlap in materials with large off-diagonal nonlinear susceptibility terms across the entire tuning range of the frequency spacing. We expect these cavities to have broad applications in the enhancement of nonlinear processes.

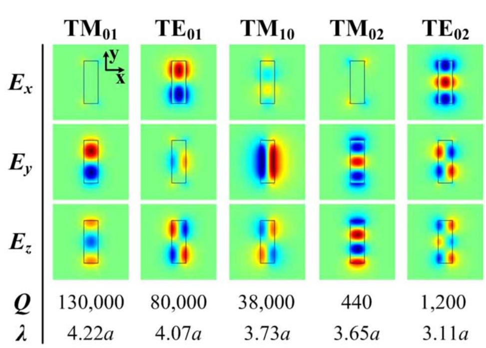

Fig. 4. (Color online) Parameters of the higher-order cavity modes for the design with $d_x=a$, $d_y=3a$.

This work was supported in part by National Science Foundation (NSF) and NSF career award. M. W. M. and I. B. B. acknowledge Natural Sciences and Engineering Research Council (Canada) for support from PDF and PGS-M fellowships. Y. Zhang dedicates this work to Jen Capell and Murray McCutcheon.

References

1. A. Faraon, I. Fushman, D. Englund, N. Stoltz, P. Petroff, and J. Vuckovic, Nat. Phys. **4**, 859 (2008).
2. M. Soljacic and J. D. Joannopoulos, Nature Mater. **3**, 211 (2004).
3. F. Raineri, C. Cojocaru, P. Monnier, A. Levenson, R. Raj, C. Seassal, X. Letartre, and P. Viktorovitch, Appl. Phys. Lett. **85**, 1880 (2004).
4. I. B. Burgess, A. W. Rodriguez, M. W. McCutcheon, J. Bravo-Abad, Y. Zhang, S. G. Johnson, and M. Loncar, Opt. Express **17**, 9241 (2009).
5. M. W. McCutcheon, D. E. Chang, Y. Zhang, M. D. Lukin, and M. Loncar, arXiv:0903.4706.
6. M. Liscidini and L. Anreani, Appl. Phys. Lett. **85**, 1883 (2004).
7. J. D. Joannopoulos, R. D. Meade, and J. N. Winn, *Photonic Crystals: Molding the Flow of Light* (Princeton Press, 1995).
8. Y. Wakayama, A. Tandaechanurat, S. Iwamoto, and Y. Arakawa, Opt. Express **16**, 21321 (2008).
9. L. C. Andreani and D. Gerace, Phys. Rev. B **73**, 235114 (2006).
10. M. Bahriz, V. Moreau, R. Colombelli, O. Crisafulli, and O. Painter, Opt. Express **15**, 5948 (2007).
11. L. A. Dunbar, V. Moreau, R. Ferrini, R. Houdre, L. Sirigu, G. Scalari, M. Giovannini, N. Hoyler, and J. Faist, Opt. Express **13**, 8960 (2005).
12. S. Hofling, J. Heinrich, H. Hofmann, M. Kamp, J. P. Reithmaier, A. Forchel, and J. Seufert, Appl. Phys. Lett. **89**, 191113 (2006).
13. M. Loncar, B. G. Lee, L. Diehl, M. A. Belkin, F. Capasso, M. Giovannini, J. Faist, and E. Gini, Opt. Express **15**, 4499 (2007).
14. P. Velha, E. Picard, T. Charvolin, E. Hadji, J. C. Rodier, P. Lalanne, and D. Peyrade, Opt. Express **15**, 16090 (2007).
15. P. B. Deotare, M. W. McCutcheon, I. W. Frank, M. Khan, and M. Loncar, Appl. Phys. Lett. **94**, 121106 (2009).
16. A. R. M. Zain, N. P. Johnson, M. Surel, and R. M. De La Rue, Opt. Express **16**, 12084 (2008).
17. Y. Zhang and M. Loncar, Opt. Express **16**, 17400 (2008).
18. M. Notomi, E. Kuramochi, and H. Taniyama, Opt. Express **16**, 11095 (2008).
19. Y. Zhang and M. Loncar, Opt. Lett. **34**, 902 (2009).
20. J. Vuckovic, M. Loncar, H. Mabuchi, and A. Scherer, IEEE J. Quantum Electron. **38**, 850 (2002).
21. K. Hennessy, C. Högerle, E. Hu, A. Badolato, and A. Imamoglu, Appl. Phys. Lett. **89**, 041118 (2006).